ЖЭТФ, 2009, том 135, вып. 5, стр. 878–884

DOUBLE PAIR PRODUCTION BY ULTRA-HIGH-ENERGY COSMIC RAY PHOTONS

***S. V. Demidov*[*], *O. E. Kalashev*[**]**

Institute for Nuclear Research, Russian Academy of Sciences
117312, Moscow, Russia

Received December 22, 2008

Using the CompHEP package, we provide a detailed estimate of the influence of double e^+e^- pair production (DPP) by photons on the propagation of ultra-high-energy electromagnetic cascades. We show that in the models where the cosmic ray photon energy reaches a few 10^3 EeV, a refined DPP analysis may lead to a substantial difference in the predicted photon spectrum compared to the previous rough estimates.

PACS: 13.85.Tp, 96.50.sh, 96.50.sb

1. INTRODUCTION

Ultra-high energy (UHE) photons have not been recognized so far by any of the present-generation experiments [1–4], although their existence is predicted by the Greisen–Zatsepin–Kuzmin effect [5, 6] as well as by most of the hypothetical top–down models of the UHE cosmic ray origin. There are several bounds on the fraction and flux of UHE photons above 10–100 EeV obtained by independent experiments [7–9]. Photon limits are used to constrain the parameters of top–down models (see, e.g., [10]). Future bounds may also limit a considerable part of the parameter space of astrophysical models in which photons are produced as secondaries from interactions of primary protons or nuclei with cosmic microwave background. Understanding interactions of UHE photons with universal backgrounds is crucial for building such constraints.

In a wide energy range, the spectra of electron and photon components of cosmic rays follow each other due to relatively rapid processes transferring γ-rays to electrons and backwards. Pair production (PP) and inverse Compton scattering (ICS) are the main processes that drive the electromagnetic cascade. In the Klein–Nishina limit $s \gg m_e^2$, either an electron or a positron produced in a pair production event typically carries almost all of the total initial energy. The produced electron (positron) then undergoes ICS, losing more than 90 % of energy, and finally the background photon carries away almost all of the initial energy of the UHE photon. Due to this cycle, the energy loss rate of the leading particle in the electromagnetic cascade is more than one order of magnitude less than the interaction rate. However, in the presence of a random extragalactic magnetic field (EGMF), the electrons may lose a substantial part of their energy by emitting synchrotron radiation. In this case, starting from a certain energy, the synchrotron loss rate for the electrons becomes dominant over the ICS rate, which leads to the suppression of the electromagnetic cascade development. Its penetration depth is then determined by the photon mean free path. Depending on the value of the EGMF, this transition may occur between ~ 1 EeV and $\sim 10^6$ EeV.

In this article, we consider a higher-order process, the e^+e^- double pair production (DPP) by photons. The DPP cross section rapidly increases with s near the threshold and quickly approaches the asymptotic value $\sigma(\infty) \approx 6.45$ μb [11–13]. The explicit energy dependence of the DPP cross section was estimated in Ref. [14] by calculating the dominant contribution from two e^+e^- pairs to the absorptive part of the gamma–gamma forward scattering amplitude. Because the PP cross section decreases with an increase in $\sqrt{s}$, the DPP rate starts to dominate over PP rate above a certain energy. For interactions with cosmic microwave background, the transition occurs above ~ 1000 EeV. In the presence of the radio background, this energy is some-

[*]E-mail: demidov@ms2.inr.ac.ru
[**]E-mail: kalashev@ms2.inr.ac.ru

what increased. If the EGMF is less than 10^{-11} G, the electromagnetic cascade still exists at these energies, and the secondary electrons from the DPP must be counted accurately. So far, electromagnetic cascade simulations such as those in [15, 16] roughly estimated the DPP effect by using the total cross section and assuming that one e^+e^- pair of the two carries all the initial energy and that two particles in the pair are produced with the same energy. Using the CompHEP package [17–19], we numerically calculate the differential cross section for the DPP and compare the effect of the DPP on propagation of an UHE electromagnetic cascade with previous estimates.

This paper is organized as follows. In Sec. 2, we present the results of the calculation of the DPP cross section. In Sec. 3, we write the transport equations for the electromagnetic cascade and calculate the coefficients for transport equations for photons and the secondary e^+ and e^- related to the DPP. In Sec. 4, we illustrate the influence of DPP in a model example. In Sec. 5, we summarize our results.

2. DOUBLE e^+e^- PAIR PRODUCTION CROSS SECTION CALCULATION

As mentioned in the Introduction, the DPP process begins to dominate over PP at very high energies $E_\gamma \gtrsim 1000$ EeV or $s \gtrsim 1$ GeV^2, which is well beyond the DPP threshold. At these and higher energies, DPP has a noticeable effect on the propagation of the electromagnetic cascade. In this energy range, the DPP total cross section is practically saturated by its asymptotic value. Therefore, we are mostly interested in the energy and angle distributions of secondary electrons (positrons) in the asymptotic regime ($s \to \infty$).

We use the CompHEP package for calculation of tree-level differential DPP cross sections. This package allows performing automatic calculations of matrix elements and their squares for any process $2 \to 2, \ldots, 2 \to 4$ at the tree level. Then, with the aid of CompHEP, we can integrate squared matrix elements over a chosen part of the multi-particle phase space (see Refs. [17–19] for the details).

We introduce a binning in the energy E^* of one of the produced electrons; here and in what follows, "$*$" denotes quantities measured in the center-of-mass frame (CMF). We then perform CompHEP simulations in the CMF and obtain distributions with respect to $\cos\Theta^*$ of the cross section in a given energy bin. Here, Θ^* is the angle between the collision axis and the momentum vector of the electron.

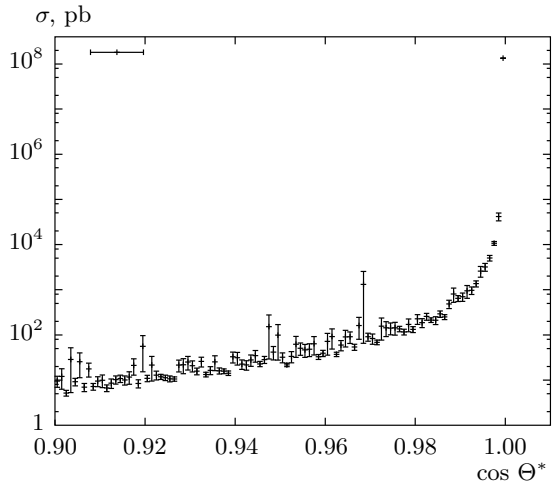

Fig. 1. Example of the distribution of the DPP cross sections with respect to $\cos\Theta^*$ for $\sqrt{s} = 10.0$ GeV in the energy E^* bin 2.25–2.5 GeV

These calculations show that the angular distribution of secondaries tends to a strongly peaked function of $\cos\Theta^*$ in the asymptotic energy range. The peaks are located at forward and backward directions, i.e., at $\cos\Theta^* = \pm 1$. This behavior is illustrated in Fig. 1 where we show an example of the angular distribution for $\sqrt{s} = 10.0$ GeV. The effect that most of the secondaries go forward or backward becomes more pronounced with an increase in $\sqrt{s}$, and in the case of a fixed $\sqrt{s}$, with a higher energy E^* of the electron. Numerically, we found that the probability of emitting a secondary electron inside the cone with $|1 - \cos\Theta^*| < 1/50$ is 96.8 % for $\sqrt{s} = 1.0$ GeV, 98.7 % for $\sqrt{s} = 2.5$ GeV, and 99.6 % for $\sqrt{s} = 10.0$ GeV. We also checked that the probability of producing two forward secondaries of the same type (e.g., when both forward particles are electrons) integrated over energies and directions of other secondaries, is of the order 10^{-3}. Hence, the main part of events consists of two e^+e^- pairs going to the opposite directions along the collision axis.

We now turn to the energy distribution. It is clear from the symmetry of the problem that the CMF energy distribution should be the same for the forward and backward electrons. We write the DPP differential cross section in the form

$$\frac{d\sigma}{dE^*} \equiv \frac{1}{\sqrt{s}}\phi\left(\frac{E^*}{\sqrt{s}/2}, s\right)\sigma_{tot}(s). \qquad (1)$$

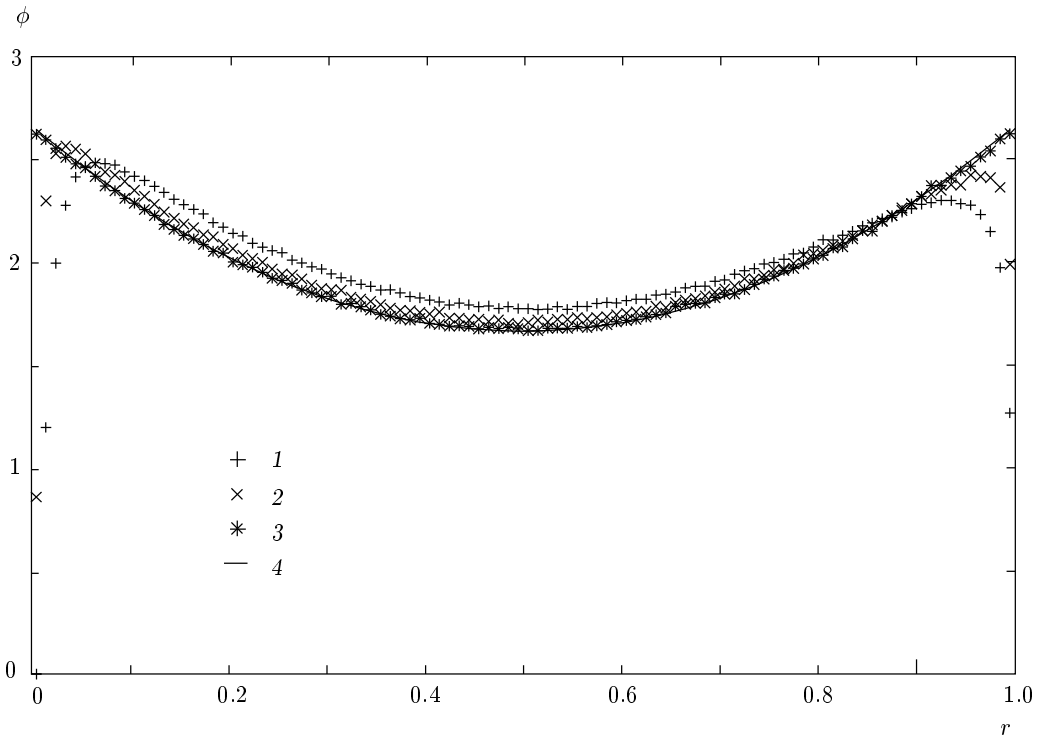

Fig. 2. The normalized energy distributions $\phi(r,s)$, $r = 2E^*/\sqrt{s}$: $\sqrt{s} = 0.1$ (*1*), 0.25 (*2*), 10.0 (*3*) GeV; and *4*, the analytic approximation in Eq. (4)

Then the energy conservation condition gives

$$\sqrt{s}\sigma_{tot}(s) = 4\int\limits_0^{\sqrt{s}/2} E^*\frac{d\sigma}{dE^*}\,dE^* = \\ = \sigma_{tot}(s)\,\sqrt{s}\int\limits_0^1 r\phi(r,s)\,dr$$

or, for any value of s,

$$\int\limits_0^1 r\phi(r,s)\,dr = 1. \qquad (2)$$

Imposing the probability conservation requirement

$$\sigma_{tot}(s) = \int\limits_0^{\sqrt{s}/2}\frac{d\sigma}{dE^*}\,dE^*$$

gives another integral constraint on $\phi(r,s)$:

$$\int\limits_0^1 \phi(r,s)\,dr = 2. \qquad (3)$$

Although conditions (2) and (3) do not necessary imply that $d\phi/ds = 0$, the results of CompHEP simulations show that for large enough s, when the cross section approaches its asymptotic value, the energy distribution of secondaries in units of the maximal energy $\sqrt{s}/2$ varies with $\sqrt{s}$ only slightly. In Fig. 2, we plot the distribution $\phi(r,s)$ as a function of r for different values of $\sqrt{s}$. It can be seen that with varying $\sqrt{s}$, the only changes in these distributions are concentrated at the borders of the plot. The distribution limit as $s \to \infty$ can be fitted (see Fig. 2) by a simple analytic expression that satisfies constraints (2) and (3):

$$\phi_{fit}(r) = \frac{5}{3} + (2r-1)^2. \qquad (4)$$

For comparison, the earlier approximation [15, 16] in terms of the distribution $\phi(r,s)$ was given by

$$\phi(r,s) = 2\delta(r-0.5). \qquad (5)$$

In our further calculations, we use Eq. (1) for the energy distribution, where $\phi(r,s) = \phi_{fit}(r)$ is given by Eq. (4), and assume that all the secondary particles are directed along the collision axis. In Sec. 4, we discuss how good the above approximation is.

3. TRANSPORT EQUATIONS

Here, we describe propagation of UHE cosmic rays using the formalism of transport equations in one dimension. Besides the DPP term on which we now focus, the full transport equations for the electrons and photons contain the terms describing ICS, PP, synchrotron radiation, and e^+e^- pair production by electrons and positrons as well as redshift terms. Below, for simplicity, we give the parts of the equations written for a nonexpanding universe with the terms related to the DPP process only:

$$\frac{d}{dt}N_e(E_e,t) = \int\limits_{E_e}^{\infty} dE_\gamma N_\gamma(E_\gamma,t) \int\limits_{\epsilon_{min}}^{\epsilon_{max}} d\epsilon\, n(\epsilon) \times \\ \times \int\limits_{-1}^{1} d\mu \frac{1-\mu}{2}\frac{d\sigma_{DPP}}{dE_e}(E_e,E_\gamma,s), \quad (6)$$

$$\frac{d}{dt}N_\gamma(E_\gamma,t) = -N_\gamma(E_\gamma,t) \int\limits_{\epsilon_{min}}^{\epsilon_{max}} d\epsilon\, n(\epsilon) \times \\ \times \int\limits_{-1}^{1} d\mu \frac{1-\mu}{2}\sigma_{DPP}(s). \quad (7)$$

Here, $N_e(E_e,t)$ is the (differential) number density of electrons at the energy E_e at time t, $n(\epsilon)$ is the number density of background photons at the energy ϵ, μ is the cosine of the collision angle ($\mu=-1$ for a head-on collision), and $s = 2E_\gamma\epsilon(1-\mu)$ is center-of-mass energy squared. The term in the right-hand side of Eq. (6) describes the influx of electrons produced in DPP. The transport equation for positrons has the same form as Eq. (6). The right-hand side of (7) describes the loss of photons due to the DPP. The factor $(1-\mu)/2$ is the flux factor. As we saw in Sec. 2, the pairs produced in DPP are directed along the collision axis. This implies that one of the pairs carries practically all the initial energy of the photon in the laboratory frame. We here neglect the nonleading pair produced in the interaction.

Replacing the integration over μ by the integration over s gives

$$\frac{d}{dt}N_e(E_e,t) = \int\limits_{E_e}^{\infty} dE_\gamma \frac{N_\gamma(E_\gamma,t)}{8E_\gamma^2} \times \\ \times \int\limits_{s_{th}}^{s_{max}} ds\, s \frac{d\sigma_{DPP}}{dE_e}(E_e;E_\gamma,s) I_\epsilon\left(\frac{s}{4E_\gamma}\right), \quad (8)$$

$$\frac{d}{dt}N_\gamma(E_\gamma,t) = -\frac{N_\gamma(E_\gamma,t)}{8E_\gamma^2} \times \\ \times \int\limits_{s_{th}}^{s_{max}} ds\, s\, \sigma_{DPP}(s) I_\epsilon\left(\frac{s}{4E_\gamma}\right), \quad (9)$$

where

$$I_\epsilon(x) = \int\limits_{x}^{\epsilon_{max}} \frac{n(\epsilon)}{\epsilon^2} d\epsilon \quad (10)$$

and $s_{th} = 16m_e^2$ is the threshold CMF energy squared for DPP and $s_{max} = 4E_\gamma\epsilon_{max}$.

We are now ready to use the results obtained in Sec. 2. We again calculate the transport equation coefficients in the limit $s \gg s_{th}$. This implies that electrons and positrons are ultrarelativistic in the CMF. The CMF γ-factor in the laboratory frame is

$$\gamma_{CMF} \equiv (1-\beta_{CMF}^2)^{-1/2} = \frac{E_\gamma}{\sqrt{s}}.$$

If the e^+ and e^- momenta are directed either toward the CMF velocity or in the opposite direction, their energy in the laboratory frame is

$$E_e = \gamma_{CMF}E_e^*(1\pm\beta_e^*) = \frac{E_\gamma}{\sqrt{s}}E_e^*(1\pm\beta_e^*),$$

where $\beta_e^* \to 1$ is electron velocity in the CMF. For the leading e^+e^- pair, we have

$$E_e = 2\frac{E_\gamma}{\sqrt{s}}E_e^*.$$

Using Eq. (1) we finally obtain

$$\frac{d}{dt}N_e(E_e,t) = \frac{1}{16}\int\limits_{E_e}^{\infty} dE_\gamma \frac{N_\gamma(E_\gamma,t)}{E_\gamma^3}\phi\left(\frac{E_e}{E_\gamma}\right) \times \\ \times \int\limits_{s_{th}}^{s_{max}} ds\, s\, \sigma_{DPP}(s) I_\epsilon\left(\frac{s}{4E_\gamma}\right). \quad (11)$$

Using numerical simulations of cosmic ray propagation presented in Sec. 4, we have also verified that utilizing the simple step function for the total cross section

$$\sigma_{DPP}(s) = \sigma_{DPP}(\infty)\Theta(s-s_{th}) \quad (12)$$

instead of the exact one listed in [14] does not introduce any visible changes to the resulting spectra. This implies that Eqs. (11) and (9) can be simplified to

$$\frac{d}{dt}N_e(E_e,t) \approx \sigma_{DPP}(\infty) \times \\ \times \int\limits_{E_e}^{\infty} dE_\gamma \frac{N_\gamma(E_\gamma,t)}{E_\gamma}\,\phi\left(\frac{E_e}{E_\gamma}\right) K_\epsilon\left(\frac{s_{th}}{4E_\gamma}\right), \quad (13)$$

$$\frac{d}{dt}N_\gamma(E_\gamma,t) \approx$$

$$\approx -2\sigma_{DPP}(\infty)N_\gamma(E_\gamma,t)K_\epsilon\left(\frac{s_{th}}{4E_\gamma}\right), \quad (14)$$

where

$$K_\epsilon(x) = \int_x^{\epsilon_{max}} I_\epsilon(y)y\,dy \quad (15)$$

is a function totally determined by the background photons spectrum.

4. MODEL EXAMPLE

In the previous sections, we found the precise expression for the distribution of secondary electrons from DPP. Here, we consider a model example to illustrate the difference introduced by the specified cross section compared to the previous estimates.

We use a numerical code developed in Ref. [15] to compute the flux of produced photons and protons. The code is based on the transport equations and calculates the propagation of nucleons, electrons, and photons using the dominant processes. For the electromagnetic cascade, it includes all the processes mentioned above. For nucleons, it accounts for single and multiple pion production, the e^+e^- pair production, and the neutron β-decay. The propagation of nucleons and the electromagnetic cascades are calculated self-consistently, that is, secondary particles produced in all reactions are propagated alongside the primaries.

In addition to cosmic microwave background, the radio, infrared, and optical components of the universal photon background are taken into account in the simulation. We note that the radio background is not yet well known. Our results strongly depend on the radio background assumed. Three models considered in this work are the estimates in [20] and the two models in [21], both predicting a larger background than the first one. For the infrared and optical background component, we used the model in [22]. This component does not have a substantial effect on the propagation of UHE protons and the electromagnetic cascade. For the strength of the random extragalactic magnetic field, we use the range of values 10^{-12} G $< B < 10^{-11}$ G following the estimate in [23].

Among the models, we chose the one in which the UHE photons contribute a substantial part of the total spectrum. We note that such models are strictly limited by the present experimental bounds on the photon component (see [10] for the details).

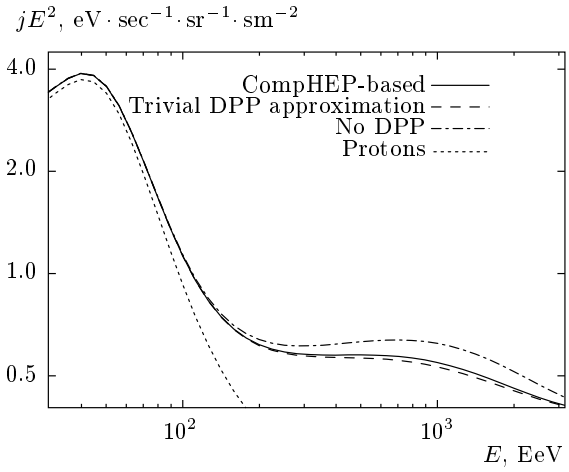

Fig. 3. Fluxes predicted by the proton emitting source described in text. The dotted line represents the proton component; solid, dashed, and dash-dotted lines represent the total flux respectively calculated with the CompHEP-based DPP, the trivial DPP estimate, and without DPP

In Fig. 3, the propagated cosmic ray flux is shown for proton sources with the spectrum

$$\frac{d\Phi}{dE} \sim E^{-1.5}, \quad E < 10^4 \text{ EeV} \quad (16)$$

homogeneously distributed in the Universe and having no evolution in the comoving frame. The spectrum presented is normalized to HiRes [3] results (fitting was done above 40 EeV). The solid line represents the total UHE cosmic ray flux calculated with the use of the new DPP estimate. The dotted line shows the proton component. The dashed line shows the total flux calculated using the earlier DPP estimate (Eq. (5)), utilizing the total cross section and assuming that one e^+e^- pair of the two carries all the initial energy and that the two particles in the pair are produced with the same energy. The dash-dotted lines are built without taking DPP into account at all.

It is clear from Fig. 3 that DPP suppresses the γ-ray flux above 100 EeV. This is only true if the minimal radio background model [20] is used. The same picture produced for any of the two models in [21] does not show any effect of DPP, because the γ flux is strongly suppressed by the PP on radio background in this case. Increasing the magnetic field above 10^{-11} G also destroys the picture, this time due to the synchrotron radiation. In the case of the minimal radio background and a moderate EGMF, the trivial DPP effect estimate leads to an extra suppression compared to the more accurate estimate proposed in this paper. However, the

overall error in terms of the integral photon flux above 100 EeV turns out to be only +7 % for the curve disregarding DPP and just −1.5 % for the trivial DPP estimate. We note that the integral photon flux fraction predicted in this model is 34 %, which is very close to the upper bound [7].

So far, we used fixed-energy distribution (4) for all values of s. We also assumed that all the secondary particles are directed along the collision axis. We now verify the accuracy of the above approximations. We repeated our simulations with energy distribution (4) replaced with the tabulated functions obtained using CompHEP for $\sqrt{s} = 1$ GeV and $\sqrt{s} = 10$ GeV. To see the maximum possible effect of the nontrivial angular distribution of secondaries, we also repeated our calculations assuming that 3.2 % of secondary particles are aligned perpendicular to the collision axis in the CMF and the rest of the particles are directed along the axis. We do not show the modified fluxes obtained in the model corresponding to Fig. 3 because they are practically indistinguishable from the curves already shown. Instead, to illustrate the maximum possible error introduced by the approximation used, we consider the pure photon sources with the same injection spectrum (16) as in Fig. 3 and count the income to the propagated electron and photon spectra from the uniformly distributed sources located within 500 Mpc from the observer. In Figs. 4 and 5, the electron and photon fluxes in this model are shown together with the fluxes calculated using the previous estimate in Eq. (5). It is clear from the figures that the previous estimate may lead to artificial features in the spectra that do not appear in our analysis. It is also clear that the discrepancy between curves 1–4 representing different versions of our analysis are small compared to the error introduced by the previous estimate. In fact, the difference between curves 1–4 is comparable to the error introduced by finite energy binning used in our numerical code.

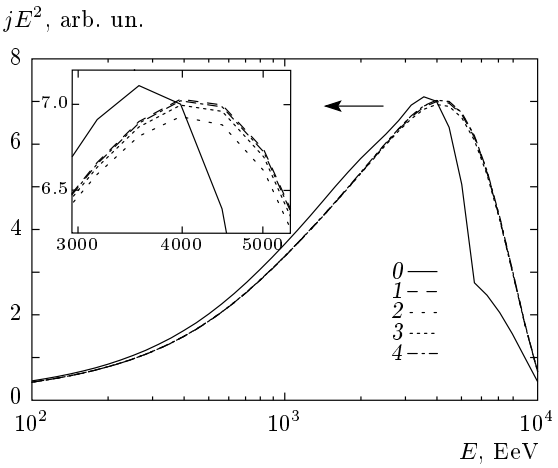

Fig. 4. Electron flux predicted by the photon emitting source described in text using: *0*, the earlier estimate in Eq. (5); *1*, the analytic fit in (4); *2*, analytic fit (4) + 3.2 % perpendicular component; *3*, $\phi(r, 1\ \text{GeV}^2)$; *4*, $\phi(r, 100\ \text{GeV}^2)$

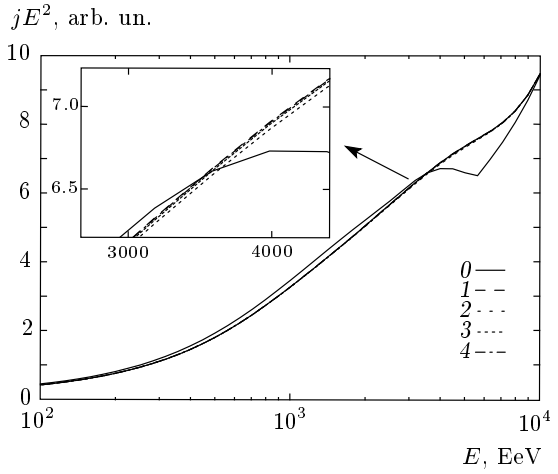

Fig. 5. The propagated photon flux predicted by the photon emitting source described in text. The notation for curves is the same as in Fig. 4

5. CONCLUSION

In this work, we have considered the DPP process in detail. We have estimated the distribution of secondary electrons and positrons and made an improved cosmic rays simulation based on the new estimate. We have shown that in certain cases, the DPP process may modify the photon component of the spectrum substantially. However, this modification can only be seen if the radio background is close to the minimal model [20] and the EGMF is lower than 10^{-11} G. In this case, there is an energy range where DPP is the main attenuation mechanism for γ rays and therefore differences in DPP estimates can be seen clearly. In the vast majority of models that do not contradict the present experimental bounds on the photon fraction in UHE cosmic rays, however, the DPP process does not make a substantial contribution to the attenuation and can therefore be treated simplistically or even disregarded.

We are indebted to D. Gorbunov for inspiring us to prepare this work. We also thank D. Semikoz for

the valuable discussions. This work was supported in part by the RFBR (grant 07-02-00820) and by the grant of the President of the Russian Federation NS-1616.2008.2, MK-1966.2008.2 (O. K.). The work of S. D. was supported in part by the grant of the Russian Science Support Foundation and the Russian Foundation for Basic Research (grants 08-02-00473-a and 08-02-00768-a). The numerical part of the work was performed on the Computational cluster of the Theoretical Division of the INR, RAS.

REFERENCES

1. M. Takeda et al., Astropart. Phys. **19**, 447 (2003); arXiv:astro-ph/0209422.
2. V. P. Egorova et al., Nucl. Phys. Proc. Suppl. **136**, 3 (2004); arXiv:astro-ph/0408493.
3. R. U. Abbasi et al. [High Resolution Fly's Eye Collaboration], Phys. Rev. Lett. **92**, 151101 (2004); arXiv:astro-ph/0208243.
4. J. Abraham et al. [Pierre Auger Collaboration], Phys. Rev. Lett. **101**, 061101 (2008); arXiv:0806.4302 [astro-ph].
5. K. Greisen, Phys. Rev. Lett. **16**, 748 (1966).
6. G. T. Zatsepin and V. A. Kuz'min, Pis'ma Zh. Eksp. Teor. Fiz. **4**, 114 (1966).
7. G. I. Rubtsov et al., Phys. Rev. D **73**, 063009 (2006); arXiv:astro-ph/0601449.
8. A. V. Glushkov, D. S. Gorbunov, I. T. Makarov, M. I. Pravdin, G. I. Rubtsov, I. E. Sleptsov, and S. V. Troitsky, Pis'ma Zh. Eksp. Teor. Fiz. **85**, 131 (2007); arXiv:astro-ph/0701245.
9. J. Abraham et al. [Pierre Auger Collaboration], Astropart. Phys. **29**, 243 (2008); arXiv:0712.1147 [astro-ph].
10. G. Gelmini, O. Kalashev, and D. V. Semikoz, Zh. Eksp. Teor. Fiz. **133**, 1214 (2008); arXiv:astro-ph/0506128.
11. H. Cheng and T. T. Wu, Phys. Rev. D **1**, 3414 (1970).
12. H. Cheng and T. T. Wu, Phys. Rev. D **2**, 2103 (1970).
13. L. N. Lipatov and G. V. Frolov, Yad. Fiz. **13**, 588 (1971).
14. R. W. Brown et al., Phys. Rev. D **8**, 3083 (1973).
15. O. E. Kalashev, V. A. Kuzmin, and D. V. Semikoz, arXiv:astro-ph/9911035; O. E. Kalashev, Ph. D. Thesis, INR RAS (2003); G. B. Gelmini, O. Kalashev, and D. V. Semikoz, J. Cosmic Astropart. Phys. **0711**, 002 (2007); arXiv:0706.2181 [astro-ph].
16. S. Lee, Phys. Rev. D **58**, 043004 (1998); arXiv:astro-ph/9604098.
17. E. Boos et al. [CompHEP Collaboration], Nucl. Instr. Meth. A **534**, 250 (2004); arXiv:hep-ph/0403113.
18. A. Pukhov et al., arXiv:hep-ph/9908288.
19. http://comphep.sinp.msu.ru.
20. T. A. Clark, L. W. Brown, and J. K. Alexander, Nature **228**, 847 (1970).
21. R. J. Protheroe and P. L. Biermann, Astropart. Phys. **6**, 45 (1996); Erratum: ibid **7**, 181 (1997).
22. F. W. Stecker, M. A. Malkan, and S. T. Scully, Astrophys. J. **648**, 774 (2006).
23. K. Dolag, D. Grasso, V. Springel, and I. Tkachev, Pis'ma Zh. Eksp. Teor. Fiz. **79**, 719 (2004); J. Cosmic Astropart. Phys. **0501**, 009 (2005).